WILEY-VCH

All-Recyclable Triboelectric Nanogenerator for Sustainable Ocean Monitoring Systems

*Junseong Ahn,[a,b§] Ji-Seok Kim,[a§] Yoonsang Jeong,[c] Soonhyoung Hwang,[b] Hyunjoon Yoo,[a] Yongrok Jeong,[a] Jimin Gu,[a] Manmatha Mahato,[a] Jiwoo Ko,[a] Sohee Jeon,[b] Ji-Hwan Ha,[a,b] Hee-Seon Seo,[d] Jungrak Choi,[a] Mingu Kang,[a] Chankyu Han,[a] Yohan Cho,[d] Chong Hyun Lee,[c] Jun-Ho Jeong,[*b] Il-Kwon Oh[*a] and Inkyu Park[*a]*

J. Ahn, J.-S. Kim, H. Yoo, Y. Jeong, J. Gu, M. Mahato, J. Ko, J.-H. Ha, J. Choi, M. Kang, C. Han, I.-K. Oh, and I. Park
Department of Mechanical Engineering, Korea Advanced Institute of Science and Technology (KAIST), Daejeon 34141, Republic of Korea
Emails: ikoh@kaist.ac.kr (I.-K. Oh), inkyu@kaist.ac.kr (I. Park)

J. Ahn, S. Hwang, S. Jeon, J.-H. Ha, and J.-H. Jeong
Department of Nano Manufacturing Technology, Korea Institute of Machinery and Materials (KIMM), Daejeon 34103, Republic of Korea
Email: jhjeong@kimm.re.kr (J.-H. Jeong)

Y. Jeong and C. H. Lee
Department of Ocean System Engineering, Jeju National University, Jeju 63243, Republic of Korea

H.-S. Seo and Y. Cho
Agency for Defense Development (ADD), Changwon 51678, Republic of Korea

§ These authors contribute equally

Keywords: recyclable triboelectric nanogenerators, renewable energy, ocean energy harvesting systems, ocean monitoring systems, intelligent buoys and life jackets

Abstract

The growing severity of environmental problems such as plastic waste and climate change has inspired the active search for solutions based on recyclable and renewable energy devices. Triboelectric nanogenerators (TENGs), which convert wasted mechanical energy into electrical energy, may offer a solution but need to be made recyclable so as to reduce or eliminate the generation of electronic waste (e-waste) upon their disposal. Herein, an all-recyclable TENG (AR-TENG) based on a thermoplastic polymer with a nanohole pattern was developed, delivering an excellent output power density of 1.547 W m^{-2} (peak output voltage = 360 V, current = 22 μA) and showing superior mechanochemical stability by maintaining its performance after immersion into seawater or 200,000 cyclic tests. The practical utility of this AR-TENG was demonstrated through its use to power a buoy-type ocean monitoring system and an intelligent life jacket, while recyclability was demonstrated by the re-fabrication of AR-TENG and the reusability in other devices was validated by successful fabrication of a plasmonic color filter. Thus, this work paves the way to the efficient harvesting of renewable energy without the concomitant production of e-waste and thus contributes to the mitigation of global environmental problems such as global warming and ozone depletion.

1. Introduction

The recent years have witnessed a revision of international standards regulating greenhouse gas (e.g., carbon dioxide) emissions and an increased interest in the substitution of fossil fuels with renewable energy sources and the recycling of artificial materials.[1,2] Accordingly, many global companies are joining environmental campaigns such as Renewable Energy 100, and renewable energy harvesting devices and recyclable electronics are attracting much attention.[3,4] Among such devices, triboelectric nanogenerators (TENGs) are of particular interest, as they harvest renewable energy by converting wasted mechanical energy into electrical energy and are particularly efficient in harvesting the renewable energy of low-frequency mechanical motions such as that of water waves and human motion.[5] However, most existing TENG devices are neither recyclable nor eco-friendly, thus yet presenting another mode of environmental pollution such as plastic and electronic wastes (e-wastes).[6]

To address this e-waste problem, researchers have explored the use of recyclable materials in the manufacture of TENG components. However, although such individual components can be reused, it is very difficult to recycle the integrated device itself since

it is composed of several composite structures and is difficult to be disassembled.[7–9] In addition, methods to disassemble such composites require complicated steps including many environmental hazards.[10] To overcome this disassembling problem, researchers have recently developed soluble TENGs in which all (or one part) of the device is completely water-soluble; this technology is, however, limited by the fact that most of electrode materials could not be recycled because they are completely decomposed.[11,12] In addition, although the combination of water and water-soluble polymers was used for recycling because of its excellent eco-friendliness, the integration of water-soluble polymers in TENG made it more vulnerable to humidity. Therefore, it is difficult to use these devices in outdoor applications or water energy harvesting (e.g., ocean energy harvesting and rain energy harvesting), which is one of the most promising applications of TENG.[13–16] In addition, the energy harvesting capacities of the currently developed recyclable TENGs are approximately 10-100 times less than those of non-recyclable TENGs because of the limitation of recyclable materials and structures.[17,18] In order to improve the performance of TENG, surface nanostructuring has been considered to increase the surface roughness and effective contact area,[19] however, poor long-term stability due to damaged patterns from repeated shear and normal impacts hindered their practical applications. Developing both durable nanopattern for high-performance TENGs and recyclable TENG devices for ecofriendliness still remains as a challenging issue.

Furthermore, systems remotely operated in ocean environments should ideally contain self-powered sensor networks to avoid the challenges associated with the periodic replacement of batteries and/or the direct measurements of ocean parameters by humans. Therefore, various buoy-type TENGs converting the motion of waves into electrical energy have been developed and used as power sources.[14,20–25] The development of mechanically and environmentally sustainable self-powered sensor networks for use in ocean environments relies on the availability of eco-friendly TENGs that have a long life span and can be stably operated for a long time.[26] However, this aspect has rarely been considered in recent studies. Conventional TENGs with micro- and nanostructured surfaces have excellent energy harvesting performance, but exhibit short life spans owing to stress concentration–induced wear.[27,28] In addition, most related studies are limited to electronics temporarily powered by a capacitor with a very fast discharge rate.[29,30] Therefore, the development of all-recyclable and disassemblable TENGs with

high-performance power generation and mechanochemical stability remains challenging. In addition, the demonstration of ocean energy harvesting and monitoring systems is highly sought.

Herein, we developed an all-recyclable and mechanochemically robust TENG (AR-TENG) with a battery charging circuit and demonstrated its application to ocean energy harvesting and monitoring systems. The developed AR-TENG based on poly(methyl methacrylate) (PMMA) with a nanohole (NH) pattern and a Pd thin film relying on three strategies. First, to realize a mechanochemically stable yet recyclable TENG, we selected PMMA and Pd as constituent materials, while a NH pattern was selected as the structure of both contacting surfaces. The above materials are not easily oxidized or dissolved in aqueous solutions, but can be disassembled in acetone, which is one of the green solvents, and thus TENG can be applied for water energy harvesting. In addition, the NH structure has a large moment of inertia against bending and a flat top surface that can uniformly distribute normal stress and is therefore mechanically stable with respect to the applied shear and normal stresses. Second, to facilitate device disassembly, we used a simple bilayer structure, which allows the entire AR-TENG to be fabricated using only two materials (i.e., PMMA and Pd). The abovementioned characteristics allowed the device to be easily disassembled and recycled by immersion into acetone. Third, to improve the energy harvesting performance of the AR-TENG, we used Pd, which shows the best triboelectric properties in combination with PMMA among noble metals, as a counter electrode, and the surface nanopatterning of PMMA was conducted by nanoimprinting lithography (NIL). The developed AR-TENG demonstrated superior energy harvesting performance, mechanochemical stability, and recyclability, delivering an output power density of 1.547 W m^{-2} with a peak output voltage of 360 V and a current of 22 μA and maintaining high performance after immersion into seawater, 200,000 cyclic tests, or re-fabrication from recycled PMMA and Pd. **Figure 1a** shows the overall fabrication, recycling, and application processes. The broad applicability and recyclability of the fabricated AR-TENG were demonstrated through its disassembly and fabrication of a plasmonic color filter (PCF) using recycled raw materials. Furthermore, we developed an energy harvesting system with a battery charging circuit capable of using the AR-TENG to charge a commercial Li-ion battery installed to drive electronics. To demonstrate the practical applicability of this energy harvesting system, we integrated it into (i) a wireless buoy-type sustainable ocean monitoring system equipped with pH, salinity, temperature, and oil leakage sensors and (ii) an intelligent life jacket that could activate a global positioning system (GPS) sensor to send a position

information signal in an emergency. The ocean monitoring system based on our AR-TENG could be operated for a long time because of its battery charging systems with a low discharge rate and high mechanochemical stability. To the best of our knowledge, this is not only the first development of the green AR-TENG with the NH pattern which has high mechanical stability, but also the first demonstration of the integrated system of the ocean energy harvesting, battery charging, and ocean monitoring systems.

2. Results and Discussion

2.1. AR-TENG Fabrication

Unlike thermosets, thermoplastic polymers are easily recyclable, as their chains do not degrade upon melting, i.e., the interactions between the chains of thermoplastic polymers are weaker than the chemical bonds between their monomer units. This property is also beneficial for structuring and design, allowing for excellent formability at temperatures above the glass transition temperature (T_g).[31] On the other hand, noble metals have outstanding chemical stability even at high temperatures and can therefore be easily extracted from integrated devices and reused. Herein, we exploited these material characteristics to fabricate the AR-TENG that utilizes a thermoplastic polymer (PMMA) as a substrate or a dielectric insulator and a noble metal (Pd) as an electrode or functional material. PMMA was selected because of its formability, chemical (water) resistance, mechanical strength, and low cost, while Pd was selected because of its chemical stability and maximized triboelectric effect in combination with PMMA (**Figure S1**). Two functional films, each comprising PMMA or Pd, were fabricated by UV-NIL, thermal NIL, and e-beam evaporation, and a simple bilayer structure was chosen to facilitate disassembly during recycling. The two bilayer films were used to construct the dielectric and conductor parts of the AR-TENG.

Figure 1b illustrates the fabrication process of functional films in more detail. To enhance the performance of the AR-TENG, we processed the PMMA film using a previously developed thermal NIL technique[31], as TENG nanopatterning enhances the triboelectric performance by significantly increasing effective contact area and surface roughness.[32–34] Initially, a Si master mold was prepared (Figure 1b-i). Then, a nanopatterned polyurethane acrylate (PUA) mold was prepared by UV-NIL (Figure 1b-ii) and used to emboss two PMMA films by thermal NIL (Figure 1b-iii). In this process, at temperatures above T_g, PMMA becomes rubbery and therefore easily deforms under

pressure. For further details regarding the fabrication process, the readers are referred to our previous research[31] and the experimental section. Subsequently, an e-beam evaporator was used to deposit a Pd thin film with a thickness of 50 nm on the back of one PMMA film (flat part) and the front of the other PMMA film (patterned part) as the electrodes of the dielectric and conductor parts of the AR-TENG, respectively (Figure 1b-iv). Figure 1c shows the photographs of the dielectric and conductor parts of the AR-TENG, while **Figures 1d and S2** show the top- and side-view scanning electron microscopy (SEM) images of the conductor part of the AR-TENG. The PMMA is patterned by thermal NIL process and Pd is deposited on both the top surface of the trench and the pillar of the nanopattern.

2.2. Structural Design and Characterization of AR-TENG

Figure 2a shows a schematic illustration of the AR-TENG, with its working mechanism and the related experimental setup presented in **Figures S3 and S4**. As discussed above, the surface nanopatterning of PMMA by thermal NIL was used to enhance the triboelectric performance, and the effects of nanopatterning on each side of the AR-TENG were investigated in detail. The peak output voltage and current of the AR-TENG with a NH pattern on only one side were 1.4–1.8 and 4.2–4.6 times higher than those of the flat-surface AR-TENG, respectively. Moreover, the peak output voltage and current of the AR-TENG with a NH pattern on both sides were 2.05–2.6 and 1.8–2.0 times higher than those of the AR-TENG with a NH pattern on only one side, respectively (Figures 2b and c). Then, the nanopattern type was optimized to achieve maximal triboelectric performance and mechanical stability. Figure 2d presents the performances of AR-TENGs with nanoline (NL), nanopillar (NP), and NH patterns, revealing that these patterns had similar positive effects, while **Figure S5** presents the top- and side-view SEM images of the above samples. However, when shear and normal forces were applied to the top surface of each pattern in the numerical simulation, the NH pattern showed the highest mechanical stability at a constant applied force per unit area (Figure 2e); the detailed simulation parameters are described in **Figure S6**. Specifically, the NH pattern exhibited the largest moment of inertia for bending and thus allowed the stress to be uniformly distributed, i.e., the amount of deformation (bending) and maximum stress were small under the applied external shear force. Therefore, when the surface morphology was observed after 200,000 cyclic tests (Figures 2f), NL and NP structures

showed permanent deformation, while the NH structure retained its original shape. The AR-TENG with the NH pattern maintained its performance during cycling, whereas in other cases, permanent deformation after 200,000 cycles resulted in a 77% decrease in the initial output voltage (Figure 2g). It is noteworthy that the NH patterned AR-TENG has excellent mechanical stability against the applied shear force, thus can maintain its superior energy harvesting performance after long-term operation of 200,000 cycles. Therefore, further experiments, including those probing the effects of applied external resistance on performance, were performed for the NH-patterned AR-TENG. As shown in Figure 2h and 2i, the peak instantaneous power density reached 1.547 W m^{-2} under an external resistance of 10 MΩ. Additionally, we evaluated the effects of the contact force and the vibration frequency of the shaker (**Figure S7**) and tested the chemical stability of the AR-TENG by immersing it into pure water and seawater which has several ions such as chloride (Cl^-), sodium (Na^+), and sulfate ($SO^2{}_4{}^-$) (Figure 2j). Neither of the two immersions affected the performance of the AR-TENG, which was ascribed to the superior chemical stability of its constituents.

2.3. Recycling of AR-TENG

Upon damage or expiry, the AR-TENG could be disassembled by simple immersion into acetone. In specific, PMMA was dissolved in acetone and reprocessed, while Pd itself was reused as a thin film form, with further details provided in **Figure S8**. Notably, all AR-TENG components, including the electrodes, could be recycled. **Figure 3** shows the results of AR-TENG recycling experiments. First, the device was decomposed into raw PMMA and Pd using the process shown in Figure S8, and the recycled PMMA and Pd were probed by Fourier-transform infrared (FTIR) spectroscopy and X-ray photoelectron spectroscopy (XPS), respectively. The FTIR spectrum of recycled PMMA showed the characteristic peaks at 1151, 1435, and 1732 cm^{-1} and was identical to that of the original PMMA (Figure 3b). The XPS spectrum of the recycled Pd showed peaks (i.e., 340 eV for Pd $3d_{3/2}$ and 335 eV for Pd $3d_{5/2}$) identical to those of original Pd metal and no additional peaks due to the chemical damages such as oxidation (e.g., 336.4 eV for PdO), which is attributed to the high chemical stability of Pd (Figure 3c). The recycled materials were used to construct AR-TENGs using the original fabrication process. As shown in Figure 3d, the performance of the re-fabricated AR-TENG was almost the same as that of the original device, with the related differences in the peak

output voltage and current equaling 1–3%. Therefore, we concluded that upon damage or expiry, the AR-TENG could be re-fabricated without the need for additional materials or the generation of waste.

Then, to demonstrate the recyclability and broad applicability of our AR-TENG, we recycled it into a PCF. Specifically, we fabricated a metallic PCF with NH arrays, as the developed method can be applied to fabricate devices with various combinations of nanopatterned PMMA and different noble metals. The working principle of the PCF is based on the extraordinary optical transmission phenomenon,[35] and the color depends on the hole size and pitch of the pattern. Therefore, a Si master mold with four different NH patterns was designed and fabricated to realize the three primary colors of light (i.e., red, green, and blue) as well as purple, which is a combination of the three primary colors (**Figure S9**). In this design, Ag was used instead of recycled Pd for the PCF because of the excellent plasmonic characteristics of the former metal, which is more conductive than Au and more resistant to oxidation by ambient air than Al.[35] **Figure S10a** illustrates the recycling of the AR-TENG, showing that it was immersed into acetone, the PMMA film was re-fabricated, and a thin Ag film was deposited by e-beam evaporation on the PUA mold. Then, nanotransfer printing (nTP) was applied instead of NIL. The previously developed nTP method was used to transfer the Ag thin film from the PUA mold to the PMMA mold at temperatures above the T_g of the latter.[32] Under these conditions, PMMA is deformed by the external pressure and mechanically interlocked with the Ag film (Figure S10a), with further details provided in our previous paper.[32] Although NIL is also suitable for PCF fabrication, it decreases the transmittance of incident light because of the inevitable formation of a metal film on both the top surface of the trench and the pillar of the nanopattern. As nTP was used herein, the Ag on the PUA pillar was transferred to the PMMA film, while the Ag on the PUA trench was not (Figure S10b). **Figure S11** presents the SEM images corresponding to each processing step and pattern. Figure 3e shows the fabricated four-color PCF, revealing sharp optical transmittance peaks (corresponding to red, green, blue, and purple) at the corresponding wavelengths (Figure 3f). The SEM images of the four different NH patterns are presented in Figure 3g. Therefore, we concluded that the AR-TENG could not only be re-fabricated but also the other optical or electrical devices such as the PCF could be fabricated using the spent AR-TENG without the need for additional materials or the generation of waste. Notably, the AR-TENG developed in this study has

a great advantage because not only it can harvest renewable ocean energy but also the device itself can be recycled without any generation of e-waste.

2.4. Characterization of Energy Harvesting System based on AR-TENG

Figures 4a and 4b show a schematic illustration and photographic images of the energy harvesting system, which comprises the large-area AR-TENG (8 cm × 8 cm), an elastomer pad, and an additional weight. Notably, the elastomer pad was used to ensure the conformal contact of each side of the large-area AR-TENG, increasing the effective contact area and thereby improving the output power of the energy harvesting system, as rigid-to-rigid surface contact dramatically reduces the actual contact area,[36] while the additional weight was used to regulate the contact condition depending on the wave amplitude, as is discussed below. The energy harvesting system was integrated into a floatable box that imitated a buoy in the ocean and floated in a wave pool (Figures 4c and S12a). In the floatable box, the AR-TENG can generate the renewable electricity by utilizing the periodic contact and separation motion between two triboelectric materials with a one-dimensional spring-mass system under the input motion of ocean waves (**Videos S1 and S2**). For improving the energy harvesting performance of the integrated buoy system, we conducted experiments with additional weights at different frequencies and amplitudes to determine the optimal conditions of the additional weights. As the mass of the extra weight increased, the peak output voltage at all of the different amplitude and frequency cases increased until a certain point and then decreased (Figure 4d). This behavior was explained by the fact that the additional weight determines the initial (neutral) distance between each side of the AR-TENG owing to the deformation of the spring. A proper weight increases the output voltage by facilitating contact with the TENG even for a small mechanical input, whereas an overly heavy weight decreases the output voltage by reducing the separation distance. Therefore, to optimize the energy harvesting system, one should consider the strong dependence of the optimized mass on the state of the wave and evaluate the effects of actuator input frequency and amplitude. Figure 4e shows the output voltages of the developed energy harvesting system when the optimal additional weight is used in various wave conditions of the wave pool. When the applied frequency was 1 Hz with the applied amplitude of 90 mm and 50 mm, the output voltage was 155 and 87 V, respectably, and when the applied frequency of 0.5

Hz with the applied amplitude of 90 mm and 50 mm, the output voltage was 28 and 6.6 V, respectively.

Then, an electrical circuit for charging a commercial Li-ion battery was developed (**Figures 4f and S12b**) and used to characterize the charging capacity of the energy harvesting system because the capacitor generally used for demonstration of TENGs has a limitation of fast discharge rate, which limits the use for the sustainable ocean monitoring system. For battery charging, the AC electrical output harvested by the AR-TENG was first converted into a DC signal by a rectifier and then used to charge a 100 μF capacitor. When the voltage of the capacitor reached 5.2 V, the electrons automatically passed through the Zener diode, and the switch connected to the regulator adopted the "on" state (Figure 4g). Subsequently, the regulator decreased the voltage to 3.3 V for the constant-voltage charging of the battery using the harvested electrical energy. As shown in Figure 4h, the voltage of battery in the initial state equaled 2.66 V, instantaneously increased to 3.3 V after connection to the regulator, and then reached 2.7 V after charging was complete. The battery voltage increase of 0.04 V upon charging means that the battery was successfully charged by electrical energy harvested by the AR-TENG, with the amount of charged energy determined as 908.22 μW·s. Notably, the regulator was also powered by the harvested energy (2.3% of the transmitted energy was consumed by the voltage drop in the regulator), i.e., the overall electrical circuit system was exclusively powered by renewable energy. The total amount of charged energy in the battery was determined from the voltage profiles of the capacitor and the battery as well as from the current profile of the regulator (**Figure S13**). A detailed discussion of battery charging capacity is provided in the Supporting Information. In addition, the developed electrical circuit could not only charge the battery, but also temporarily operate a commercial Arduino board (Figure S12b), and was therefore deemed to be a suitable self-powered microcontroller system capable of operating wireless sensors and periodically transmitting signals for a sustainable ocean monitoring system.

The battery charging demonstration of the proposed energy harvesting system based on AR-TENG could pave the way for sustainable operation of renewable energy. In addition, the output power can be improved by arranging multiple AR-TENGs with mechanically robust and high-performance properties in the ocean for sensor networks of the ocean monitoring system

2.5. Applications of the AR-TENG to the Ocean Monitoring Systems

To demonstrate the practical applicability of the developed energy harvesting system, we integrated it into a buoy-type ocean monitoring system and a life jacket. The intelligent buoy was designed to monitor the condition of seawater and to regularly transmit it to land through wireless communication, comprising the AR-TENG with a battery charging module, a wireless communication module, and four (pH, salinity, temperature, and oil leakage) sensors (**Figures 5a and 5b**). Among these four sensors, three of them (pH-, salinity-, and temperature sensors) measure the representative monitoring parameters of seawater, and the other (oil leak sensors) detects the oil leakage from vessels on the sea. As shown in Figure 5c and **Video S3**, each parameter was successfully measured by the sensors when brine, acidic buffer solution, hot water, and oil were successively added to the seawater. The intelligent life jacket capable of automatically or manually transmitting an emergency signal (Figure 5d) comprised the AR-TENG, a battery-charging module, a wireless communication module, and an integrated GPS sensor (Figure 5e). In this case, the AR-TENG could be operated not only by ocean wave energy, but also by human motion (Figure 5f). When the Zener diode switch was turned on, i.e., when the life jacket floated on seawater or was activated manually, the GPS sensor transmitted an emergency signal including location details (Figure 5g and **Video S4**). Thus, the developed energy harvesting system was found to hold great promise for ocean monitoring systems (e.g., intelligent buoys and life jackets).

3. Conclusions

In this study, a high-performance and mechanochemically stable AR-TENG was developed and used to fabricate a sustainable ocean energy harvesting system. The AR-TENG successfully secured the excellent mechanical and chemical durability by designing the NH structure with a large moment of inertia against bending and applying chemically stable materials, respectively. To the best of our knowledge, this AR-TENG is the first to be ever reported, exhibiting the highest performance and durability among the known recyclable or disposable TENGs (**Table S1**). In addition, as the AR-TENG contained only a thermoplastic polymer (PMMA) and a noble metal (Pd), the entire device, including electrodes, could be easily disassembled in acetone and recycled to

reduce the generation of e-waste. Moreover, the AR-TENG could be recycled as a PCF using the nTP method, and the obtained PCF demonstrated four clear colors, namely red, green, blue, and purple. Then, the AR-TENG was subsequently integrated into a buoy-type ocean monitoring system and an intelligent life jacket. The intelligent buoy included four different sensors and could monitor oil leakage as well as the pH, salinity, and temperature of seawater, while the intelligent life jacket contained a GPS sensor and could notify an emergency of the wearer to land. In both cases, the battery was continuously charged by the energy supplied by the AR-TENG for a sustainable operation of the ocean monitoring system.

Despite the above success, there are still some challenges to be addressed. First, a more environmentally friendly combination of polymers and solutions needs to be developed without degrading the performance. Although acetone is a preferred green solvent,[37] even in the pharmaceutical industry, it is still somewhat toxic.[38] Therefore, the development of AR-TENGs that can be recycled in a more environmentally friendly way will help to reduce the generation of chemical waste. Second, the realization of a perfect AR-TENG requires the availability of recyclable electric wires and packing materials. Herein, recycling was limited to polymers and electrodes on the TENG structure and was not applied to the electric wires and packaging materials. Nevertheless, we believe that the results presented herein will help to resolve global environmental problems such as climate change[39,40] and ozone depletion through the efficient and green harvesting of wasted mechanical energy and expect them to pave the way to the harvesting of renewable energy beyond that of oceans, e.g., wind and rain energy.

4. Experimental

AR-TENG fabrication and recycling: A Si master was prepared by krypton fluoride (KrF) lithography to fabricate functional films comprising nanopatterned PMMA and Pd thin films. For polymer mold replication, RM-311 resin (polyurethane, Minuta Technology Co., Ltd., Korea) was poured onto the prepared Si master and covered by a UV-transparent polyethylene terephthalate film. Pressure was applied to the resin using a hand roller to facilitate the complete penetration of this resin into the nanopatterns of the Si master. Then, the resin was cured under illumination with UV light and separated from the Si master to afford a polymer mold. This process could be conducted repeatedly, and various nanopatterns could be fabricated using

various Si masters. The detailed fabrication of the polymer mold from the Si master is described in our previous work.[41] Note that the surface of the Si master had to be treated with trichloro(1H,1H,2H,2H-perfluorooctyl)silane to facilitate polymer mold detachment. Then, the nanopatterned PUA mold was used to pattern the PMMA film at 110 °C (i.e., at a temperature above the T_g of PMMA) and 5 bar for 10 min. Two nanopatterned PMMA films were fabricated using repeated NIL. Next, a 50-nm thick Pd layer was deposited using an e-beam evaporator (Daeki Hi-Tech Co., Ltd., Korea) on one side of both films: One layer was deposited on the back of the PMMA film (flat part) and the other was deposited on the front of the other PMMA film (patterned part) to afford the electrodes of the dielectric and conductor parts of the AR-TENG, respectively. The two functional films were used on each side of the AR-TENG, and both films comprising PMMA and Pd (total thickness = 30 μm) were attached to a thick PMMA substrate (thickness = 1 mm), and electric wires were connected using Ag paste. The fabricated samples were evaluated by field-emission scanning electron microscopy (FE-SEM; Sirion, FEI, the Netherlands) and focused ion-beam scanning electron microscopy (FIB-SEM; Helios Nanolab, FEI, the Netherlands). For recycling, the AR-TENG was detached from the thick PMMA substrate, and the two functional films were immersed into acetone for 20 min. The floated Pd film was removed using a tweezer and reused as a source for the e-beam evaporation. The remaining acetone solution of PMMA was placed in a vacuum oven and heated for 5 h at 50 °C to evaporate acetone. The remaining PMMA was reformed as a thin film by repeated hot-pressing at 140–200 °C and 3–5 bar for a new thermal NIL process.

AR-TENG characterization: Characterization was performed for a device with dimensions of 3 cm × 3 cm. A digital phosphor oscilloscope (DPO2002B, Tektronix, USA), a high-voltage probe with an input impedance of 40 MΩ (P5100A, Tektronix, USA), and a pre-current amplifier (SR570, Stanford Research Systems, USA) were used to measure the output voltage and current. A system electrometer (Model 6514, Keithley Instrument, USA) was used to measure the output voltage, current, and transferred charge. A dual-channel arbitrary function generator (AFG3022, Tektronix, USA) was used to generate a sinusoidal function for shaker excitation. As a high voltage and current were required to drive the shaker, a power amplifier (Type BAA 120, TIRA, Germany) was used. A vibration test system (TV 51075, TIRA, Germany) was used as a shaker to demonstrate the contact-separation mode of the AR-TENG. Contact force measurements were performed using a force sensor (1051V2, Dytran Instruments, USA) powered by a sensor signal conditioner (Model 480E09, PCB Piezotronics, USA). The

output triboelectric performance of the AR-TENG was investigated at different forces (1, 2, 4, 6, and 8 N) and frequencies (1–7 Hz), as shown in Figure S7. Thereafter, triboelectric performance was characterized at an operating force of 8 N and a frequency of 5 Hz. The finite element method was used in conjunction with COMSOL Multiphysics software to compare the mechanical stabilities of PMMA films with different surface morphologies (NL, NP, and NH patterns). For comparison, the unit cell size was set to 0.9 μm × 0.9 μm, the same normal and shear force per unit area were set to be exerted on the surface, and the von Mises stress was compared.

Recycling and PCF fabrication: The PCF was fabricated using previously developed NIL and nTP processes, with AR-TENG recycling performed as described above. The nTP process was conducted using the recycled PMMA film and Ag pellets. A Si master mold with four different NH pattern types was designed and fabricated by KrF lithography, and a nanopatterned PUA replica was prepared by the abovementioned process for PUA mold fabrication. Then, a 40-nm-thick layer of Ag was deposited on the PUA mold using an e-beam evaporator. The nanopatterned PUA mold with Ag was transferred onto the PMMA film using a previously developed nTP technique, namely heating above the T_g of PMMA (110 °C) at 6 bar for 5 min. After 5-min cooling, the PUA mold was separated from the PMMA film to obtain an Ag nanopattern on the PMMA film (i.e., the PCF). The optical transmittance of the resulting PCF was characterized using a spectrometer (QE Pro 6000, Ocean Optics, USA).

Fabrication and characterization of the ocean energy harvesting system with a battery charging circuit: Each NH-patterned thin film comprising PMMA and Pd (total thickness = 30 μm) was attached to the thick PMMA substrate for proper rigidity. A simple mechanical spring system utilizing an AR-TENG with a size of 8 cm × 8 cm was designed to harvest ocean wave energy. A soft elastomer pad fabricated using Ecoflex (Ecoflex 0030, Smooth-On, USA) was placed on one side of the AR-TENG for a conformal contact. A mechanical spring and an additional weight were systematically used throughout the experiments. The output voltages of the ocean energy harvesting system with a battery charging circuit were examined in the wave pool with the size of 11 × 10 m. In this experiment, the performance of the developed harvesting system was evaluated as functions of the amplitude (50 and 90 mm) and frequency (0.5 and 1 Hz) of the actuator which generates the water wave (Figure S12a).

An ultralow power step-down regulator with input voltage monitoring and regulation functions (ADP5304, Analog Devices, USA) was used to charge a commercial Li-ion battery (MS621FE, Seiko Instruments Micro Energy, Japan) with a nominal capacity of 5.5 mAh using a constant-voltage charging method. The regulator converted the irregular output voltage of the capacitor into a constant voltage. In addition, a Zener diode (TZX3V0B-TR, Vishay Semiconductors, USA) was used to adjust the threshold voltage of a switch connected to the regulator to 5.2 V.

Construction of the ocean monitoring system*:* The ocean monitoring system was constructed using an Arduino Uno board, a Bluetooth module (HC-05), the customized battery charging circuit, the AR-TENG, and additional sensors. For the intelligent buoy, a salinity sensor (Vernier, USA), a pH sensor (Vernier, USA), a temperature sensor (DS18B20), and an oil leakage sensor (LK16-T2-2000HD, YUMINST, Korea) were used, while a GPS sensor (GY-NEO6MV2) was used for the intelligent life jacket.

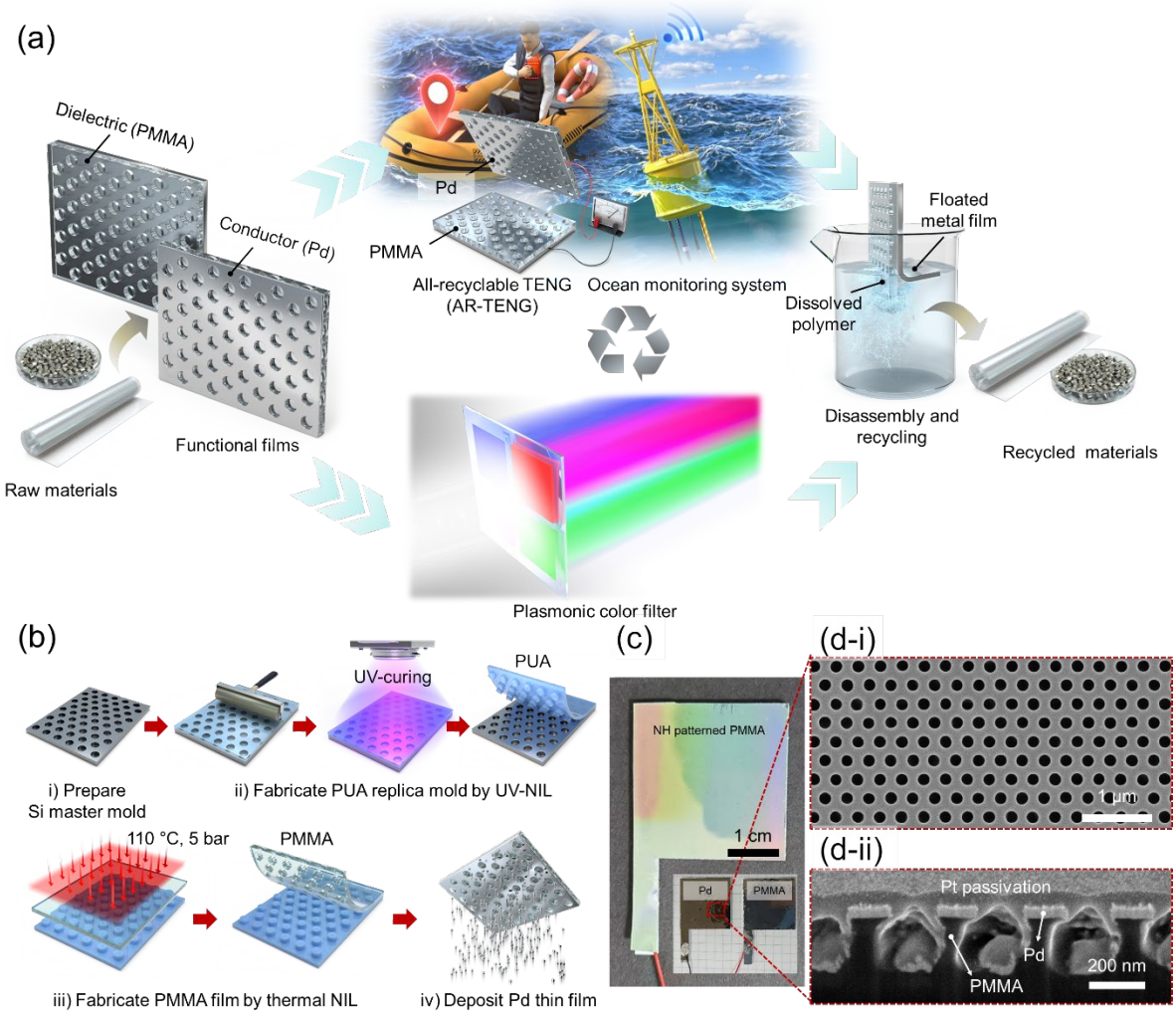

Figure 1. Schematic illustration of (a) the AR-TENG recycling process and (b) functional film fabrication by UV- and thermal NIL. (c) Photographic images of the fabricated AR-TENG, with inset showing its dielectric (PMMA) and conductor (Pd) parts. The iridescent color different from the color of the surface material (PMMA) verifies the formation of periodic nanostructures on the surface. (d-i) Top- and (d-ii) side-view SEM images of the conductor part of the AR-TENG. For the acquisition of the side-view image, the sample was sliced using a focused ion beam.

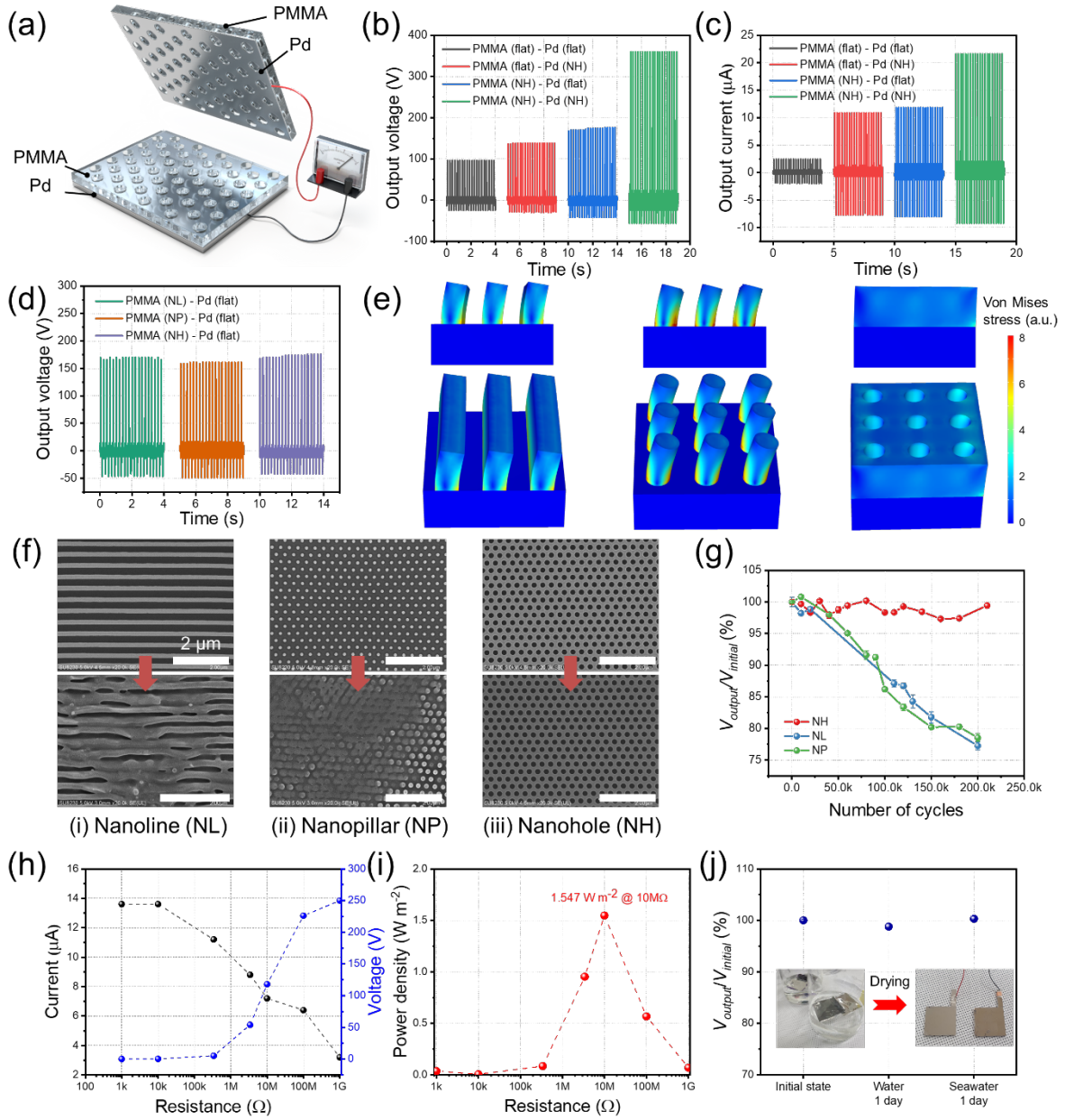

Figure 2. (a) Schematic illustration of the developed AR-TENG. (b) Output voltage and (c) output current obtained for different surface morphologies on each AR-TENG side. (d) Output voltages of one-side-nanopatterned AR-TENGs with NL, NP, and NH patterns. (e) Results of mechanical stress analysis under uniform shear and normal stress obtained by numerical simulation for different nanopatterns using the finite element method. Effects of cyclic contacts on (f) top-view SEM images of AR-TENGs with different patterns and (g) the output voltage divided by the initial output voltage before and after 200,000 cycles. In the mechanical stability test, the AR-TENGs with the nanopatterns on both conductor and dielectric sides were used. (h) Voltage and current and (i) the corresponding power density of the NH-patterned AR-TENG as functions of

applied external resistance. (j) Effects of immersion into deionized water and seawater for 1 day on the output voltage of the NH-patterned AR-TENG.

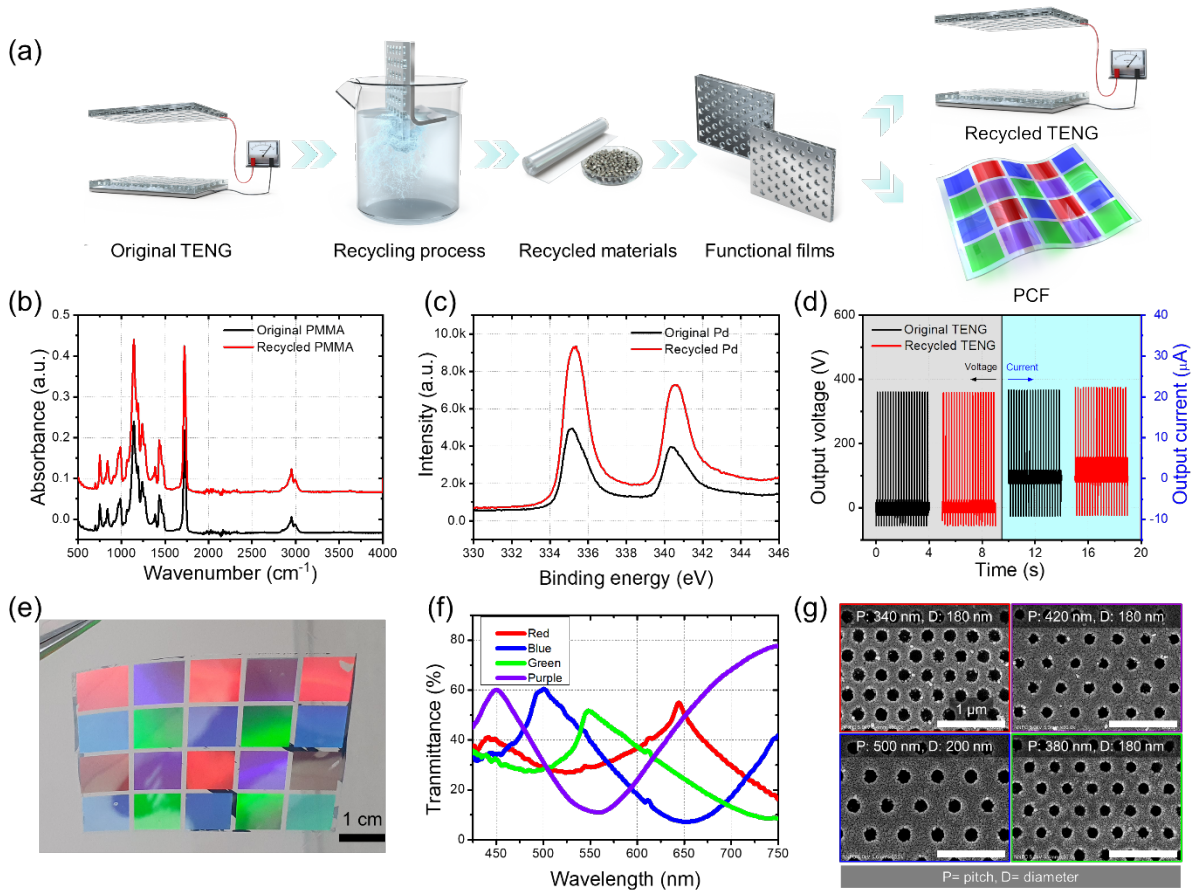

Figure 3. (a) Schematic illustration of the AR-TENG recycling process involving disassembly and re-assembly for re-fabrication of the AR-TENG and PCF. (b) FTIR spectra of the PMMA film recorded before and after recycling. (c) XPS spectra of Pd recorded before and after recycling. Effects of recycling on (d) the output voltage and the current of the AR-TENG. (e) Photographic image and (f) transmittance spectra of the fabricated four-color PCF. (g) Top-view SEM images of the four different PCF regions representing different colors.

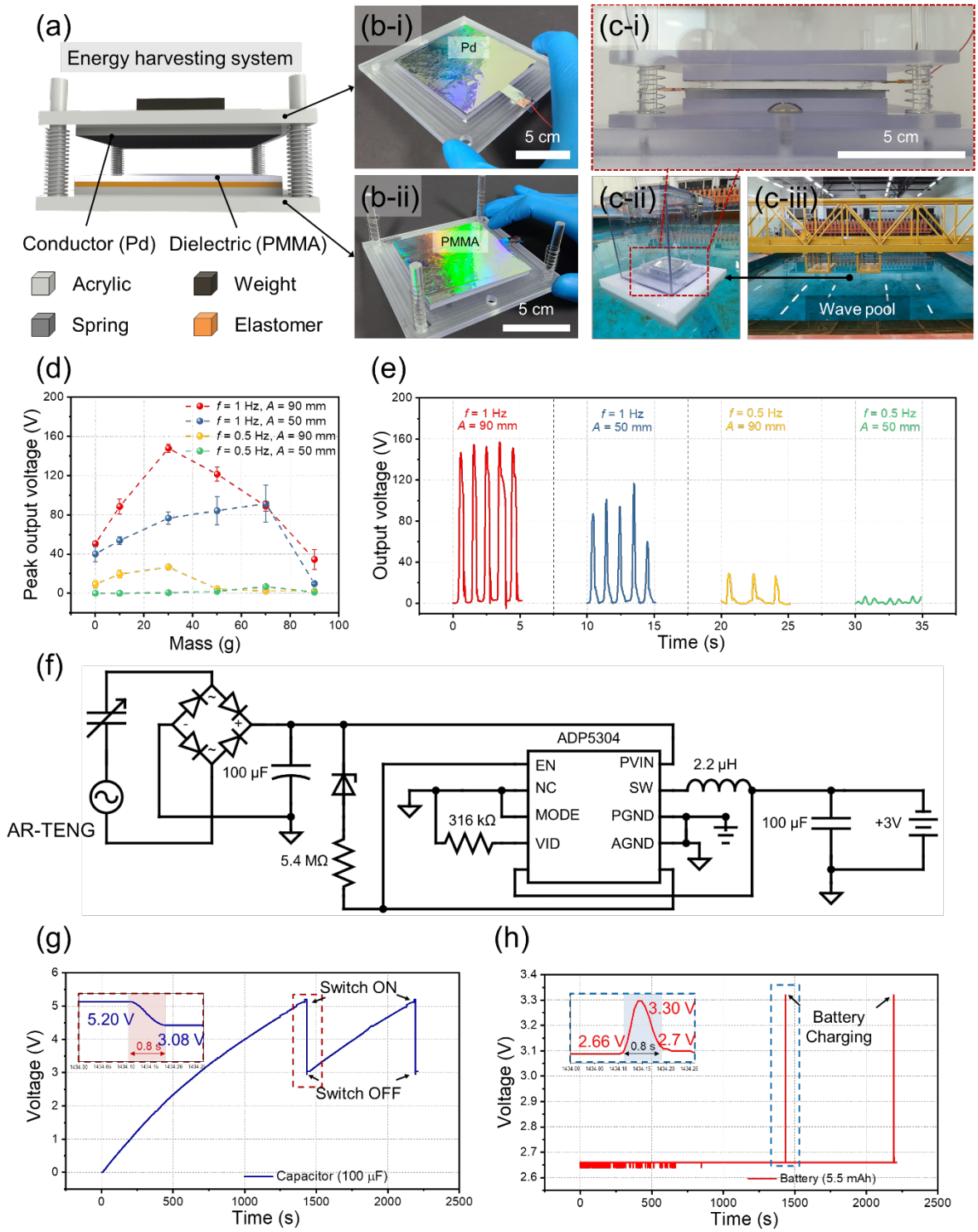

Figure 4. (a) Schematic illustration and (b) photographic images of the developed ocean energy harvesting system. (c) Photographic images of the developed system in a wave pool capable of generating water waves to mimic ocean environments. (d) Peak output voltages of the energy harvesting system obtained for various weights under diverse wave conditions generated at different actuator frequencies (*f*) and amplitudes (*A*). (e) Output voltages using optimal weights in various wave conditions. (f) Electrical circuit

used to charge a commercial Li-ion battery or drive a commercial Arduino board at a constant voltage. The voltage profiles of (g) the capacitor and (h) the battery upon constant charging by the AR-TENG.

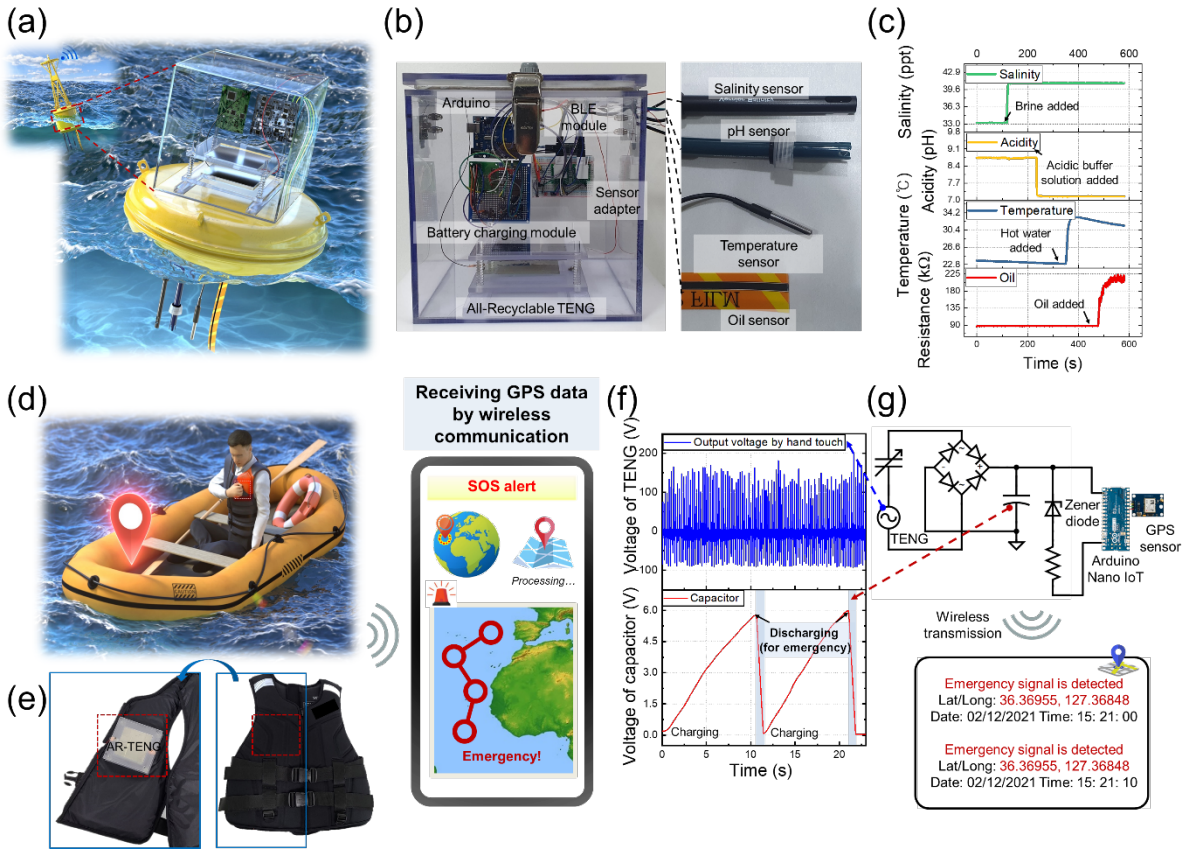

Figure 5. (a) Schematic illustration and (b) photographic images of the intelligent buoy including a battery charging module, a wireless communication module, and four (pH, salinity, temperature, and oil leakage) sensors. (c) Results of intelligent buoy evaluation under different ocean conditions. In this experiment, brine, acidic buffer solution, hot water, and oil were added to the seawater successively. (d) Schematic illustration and (e) photographic images of the intelligent life jacket including the AR-TENG, a battery-charging module, a wireless communication module, and a GPS sensor. (f) The voltage of the AR-TENG by hand touch and capacitor integrated into the intelligent life jacket. (g) Schematic illustration of the electrical circuit for triggering the GPS sensor using the harvested energy by the AR-TENG and the screen of a mobile device which can receive the GPS data from the intelligent life jacket by wireless communication.

Conflicts of Interest

There are no conflicts to declare.

Supporting Information

Supporting Information is available from the Wiley Online Library or from the author.

Acknowledgments

J. Ahn and J.-S. Kim contributed equally to this work. This work was supported by Creative Research Initiative Program (2015R1A3A2028975) and funded by National Research Foundation of Korea (NRF), the Defense Acquisition Program Administration and the Agency for Defense Development (ADD) in Korea under the contract UD200011DD, by the Center for Advanced Meta-Materials (CAMM) funded by the Ministry of Science, ICT, and Future Planning as Global Frontier Project (CAMM No. 2014M3A6B3063707), Institute of Information & Communications Technology Planning & Evaluation (IITP) grant funded by the Korea government (MSIT) (No. 2020-0-00914, Development of hologram printing downsizing technology based on holographic optical element(HOE)), and by a National Research Foundation of Korea (NRF) grant funded by the Korea government (MSIT) [No. 2021R1A2C3008742]. This research was a part of the project titled 'Development of Management Technology for HNS Accident' (No. D11502815H480000140 2015034016), funded by the Ministry of Oceans and Fisheries, Korea.

Received: ((will be filled in by the editorial staff))
Revised: ((will be filled in by the editorial staff))
Published online: ((will be filled in by the editorial staff))

References

[1] J. Yu, X. Wang, M. Zhou, Q. Wang, *Energy Environ. Sci.* **2019**, *12*, 2672.

[2] M. Amer, E. Z. Wojcik, C. Sun, R. Hoeven, R. Hoeven, J. M. X. Hughes, M. Faulkner, I. S. Yunus, S. Tait, L. O. Johannissen, S. J. O. Hardman, D. J. Heyes, G. Q. Chen, G. Q. Chen, M. H. Smith, P. R. Jones, H. S. Toogood, N. S. Scrutton, N. S. Scrutton, N. S. Scrutton, *Energy Environ. Sci.* **2020**, *13*, 1818.

[3] N. A. Shepelin, P. C. Sherrell, E. Goudeli, E. N. Skountzos, V. C. Lussini, G. W. Dicinoski, J. G. Shapter, A. V. Ellis, *Energy Environ. Sci.* **2020**, *13*, 868.

[4] O. J. Guerra, J. Eichman, P. Denholm, *Energy Environ. Sci.* **2021**, *14*, 5132.

[5] C. Rodrigues, D. Nunes, D. Clemente, N. Mathias, J. M. Correia, P. Rosa-Santos, F. Taveira-Pinto, T. Morais, A. Pereira, J. Ventura, *Energy Environ. Sci.* **2020**, *13*, 2657.

[6] M. Heacock, C. B. Kelly, K. A. Asante, L. S. Birnbaum, Å. L. Bergman, M. N. Bruné, I. Buka, D. O. Carpenter, A. Chen, X. Huo, M. Kamel, P. J. Landrigan, F. Magalini, F. Diaz-Barriga, M. Neira, M. Omar, A. Pascale, M. Ruchirawat, L. Sly, P. D. Sly, M. van den Berg, W. A. Suk, *Environ. Health Perspect.* **2016**, *124*, 550.

[7] Z. Bai, Y. Xu, J. Li, J. Zhu, C. Gao, Y. Zhang, J. Wang, J. Guo, *ACS Appl. Mater. Interfaces* **2020**, *12*, 42880.

[8] S. Parandeh, M. Kharaziha, F. Karimzadeh, *Nano Energy* **2019**, *59*, 412.

[9] L. Zhang, Y. Liao, Y. C. Wang, S. Zhang, W. Yang, X. Pan, Z. L. Wang, *Adv. Funct. Mater.* **2020**, *30*, 1.

[10] L. Chen, C. Yu, C. Shen, C. Zhang, L. Liu, K. Shen, X. Tang, Y. Chen, *J. Soils Sediments* **2010**, *10*, 359.

[11] Y. Lu, X. Li, J. Ping, J. song He, J. Wu, *Adv. Mater. Technol.* **2020**, *5*, 1.

[12] Q. Liang, Q. Zhang, X. Yan, X. Liao, L. Han, F. Yi, M. Ma, Y. Zhang, *Adv. Mater.* **2017**, *29*.

[13] W. Xu, H. Zheng, Y. Liu, X. Zhou, C. Zhang, Y. Song, X. Deng, M. Leung, Z. Yang, R. X. Xu, Z. L. Wang, X. C. Zeng, Z. Wang, *Nature* **2020**, *578*, 392.

[14] X. Liang, T. Jiang, G. Liu, Y. Feng, C. Zhang, Z. L. Wang, *Energy Environ. Sci.* **2020**, *13*, 277.

[15] L. Xu, L. Xu, J. Luo, Y. Yan, B. E. Jia, X. Yang, Y. Gao, Z. L. Wang, *Adv. Energy Mater.* **2020**, *10*, 1.

[16] S. Nie, H. Guo, Y. Lu, J. Zhuo, J. Mo, Z. L. Wang, *Adv. Mater. Technol.* **2020**, *5*, 1.

[17] Q. Zheng, Y. Zou, Y. Zhang, Z. Liu, B. Shi, X. Wang, Y. Jin, H. Ouyang, Z. Li, Z. L. Wang, *Sci. Adv.* **2016**, *2*, 1.

[18] J. Zhang, S. Hu, Z. Shi, Y. Wang, Y. Lei, J. Han, Y. Xiong, J. Sun, L. Zheng, Q. Sun, G. Yang, Z. L. Wang, *Nano Energy* **2021**, *89*, 106354.

[19] Q. Zhou, K. Lee, K. N. Kim, J. G. Park, J. Pan, J. Bae, J. M. Baik, T. Kim, *Nano Energy* **2019**, *57*, 903.

[20] G. Knutsen, *Mar. Pollut. Bull.* **1983**, *14*, 112.

[21] K. Xia, J. Fu, Z. Xu, *Adv. Energy Mater.* **2020**, *10*, 1.

[22] H. Wang, Z. Fan, T. Zhao, J. Dong, S. Wang, Y. Wang, X. Xiao, C. Liu, X. Pan, Y. Zhao, M. Xu, *Nano Energy* **2021**, *84*, 105920.

[23] L. Liu, X. Yang, L. Zhao, H. Hong, H. Cui, J. Duan, Q. Yang, Q. Tang, *ACS Nano* **2021**, *15*, 9412.

[24] G. Liu, H. Guo, S. Xu, C. Hu, Z. L. Wang, *Adv. Energy Mater.* **2019**, *9*, 1.

[25] M. Xu, T. Zhao, C. Wang, S. L. Zhang, Z. Li, X. Pan, Z. L. Wang, *ACS Nano* **2019**, *13*, 1932.

[26] Z. L. Wang, T. Jiang, L. Xu, *Nano Energy* **2017**, *39*, 9.

[27] P. Chen, J. An, S. Shu, R. Cheng, J. Nie, T. Jiang, Z. L. Wang, *Adv. Energy Mater.* **2021**, *11*, 1.

[28] X. Wei, Z. Zhao, C. Zhang, W. Yuan, Z. Wu, J. Wang, Z. L. Wang, *ACS Nano* **2021**, *15*, 13200.

[29] D. Y. Kim, H. S. Kim, D. S. Kong, M. Choi, H. B. Kim, J. H. Lee, G. Murillo, M. Lee, S. S. Kim, J. H. Jung, *Nano Energy* **2018**, *45*, 247.

[30] D. Zhang, J. Shi, Y. Si, T. Li, *Nano Energy* **2019**, *61*, 132.

[31] Z. J. Zhao, J. Ahn, S. H. Hwang, J. Ko, Y. Jeong, M. Bok, H. J. Kang, J. Choi, S. Jeon, I. Park, J. H. Jeong, *ACS Nano* **2021**, *15*, 503.

[32] J. Ahn, Z. J. Zhao, J. Choi, Y. Jeong, S. Hwang, J. Ko, J. Gu, S. Jeon, J. Park, M. Kang, D. V. Del Orbe, I. Cho, H. Kang, M. Bok, J. H. Jeong, I. Park, *Nano Energy* **2021**, *85*, 105978.

[33] A. Šutka, K. Malnieks, L. Lapčinskis, P. Kaufelde, A. Linarts, A. Berziņa, R. Zabels, V. Jurķans, I. Gorņevs, J. Blums, M. Knite, *Energy Environ. Sci.* **2019**, *12*, 2417.

[34] H. S. Wang, C. K. Jeong, M. H. Seo, D. J. Joe, J. H. Han, J. B. Yoon, K. J. Lee, *Nano Energy* **2017**, *35*, 415.

[35] S. H. Hwang, Z. J. Zhao, S. Jeon, H. Kang, J. Ahn, J. H. Jeong, *Nanoscale* **2019**, *11*, 11128.

[36] Y. Chen, X. Pu, M. Liu, S. Kuang, P. Zhang, Q. Hua, Z. Cong, W. Guo, W. Hu, Z. L. Wang, *ACS Nano* **2019**, *13*, 8936.

[37] G. Szekely, M. F. Jimenez-Solomon, P. Marchetti, J. F. Kim, A. G. Livingston, *Green Chem.* **2014**, *16*, 4440.

[38] D. Prat, J. Hayler, A. Wells, *Green Chem.* **2014**, *16*, 4546.

[39] L. Pan, E. M. Powell, K. Latychev, J. X. Mitrovica, J. R. Creveling, N. Gomez, M. J. Hoggard, P. U. Clark, *Sci. Adv.* **2021**, *7*, 27.

[40] R. I. Woolway, E. Jennings, T. Shatwell, M. Golub, D. C. Pierson, S. C. Maberly, *Nature*

2021, *589*, 402.

[41] Z. J. Zhao, J. Ahn, J. Ko, Y. Jeong, M. Bok, S. H. Hwang, H. J. Kang, S. Jeon, J. Choi, I. Park, J. H. Jeong, *ACS Appl. Mater. Interfaces* **2021**, *13*, 3358.

ToC (Table of Contents)

All-Recyclable Triboelectric Nanogenerator for Sustainable Ocean Monitoring Systems

*Junseong Ahn,[a,b§] Ji-Seok Kim,[a§] Yoonsang Jeong,[c] Soonhyoung Hwang,[b] Hyunjoon Yoo,[a] Yongrok Jeong,[a] Jimin Gu,[a] Manmatha Mahato,[a] Jiwoo Ko,[a] Sohee Jeon,[b] Ji-Hwan Ha,[a,b] Hee-Seon Seo,[d] Jungrak Choi,[a] Mingu Kang,[a] Chankyu Han,[a] Yohan Cho,[d] Chong Hyun Lee,[c] Jun-Ho Jeong,[*b] Il-Kwon Oh[*a] and Inkyu Park[*a]*

Keywords: recyclable triboelectric nanogenerators, renewable energy, ocean energy harvesting systems, ocean monitoring systems, intelligent buoys and life jackets

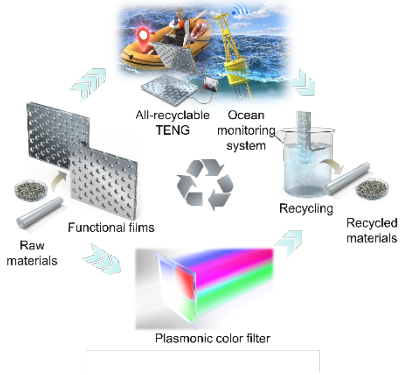

All-recyclable triboelectric nanogenerator (AR-TENG) that exhibits high power density and excellent mechanochemical stability is developed. The recyclability is demonstrated through its disassembly and fabrication of plasmonic color filter. Ocean energy harvesting system based on AR-TENG is developed and is used to power buoy-type ocean monitoring system and intelligent life jacket.

Supporting Information

All-Recyclable Triboelectric Nanogenerator for Sustainable Ocean Monitoring Systems

*Junseong Ahn,[a,b§] Ji-Seok Kim,[a§] Yoonsang Jeong,[c] Soonhyoung Hwang,[b] Hyunjoon Yoo,[a] Yongrok Jeong,[a] Jimin Gu,[a] Manmatha Mahato,[a] Jiwoo Ko,[a] Sohee Jeon,[b] Ji-Hwan Ha,[a,b] Hee-Seon Seo,[d] Jungrak Choi,[a] Mingu Kang,[a] Chankyu Han,[a] Yohan Cho,[d] Chong Hyun Lee,[c] Jun-Ho Jeong,[*b] Il-Kwon Oh[*a] and Inkyu Park[*a]*

J. Ahn, J.-S. Kim, H. Yoo, Y. Jeong, J. Gu, M. Mahato, J. Ko, J.-H. Ha, J. Choi, M. Kang, C. Han, I.-K. Oh, and I. Park
Department of Mechanical Engineering, Korea Advanced Institute of Science and Technology (KAIST), Daejeon 34141, Republic of Korea
Emails: ikoh@kaist.ac.kr (I.-K. Oh), inkyu@kaist.ac.kr (I. Park)

J. Ahn, S. Hwang, S. Jeon, J.-H. Ha, and J.-H. Jeong
Department of Nano Manufacturing Technology, Korea Institute of Machinery and Materials (KIMM), Daejeon 34103, Republic of Korea
Email: jhjeong@kimm.re.kr (J.-H. Jeong)

Y. Jeong and C. H. Lee
Department of Ocean System Engineering, Jeju National University, Jeju 63243, Republic of Korea

H.-S. Seo and Y. Cho
Agency for Defense Development (ADD), Changwon 51678, Republic of Korea

§ These authors contribute equally

Keywords: recyclable triboelectric nanogenerators, renewable energy, ocean energy harvesting systems, ocean monitoring systems, intelligent buoys, intelligent life jackets

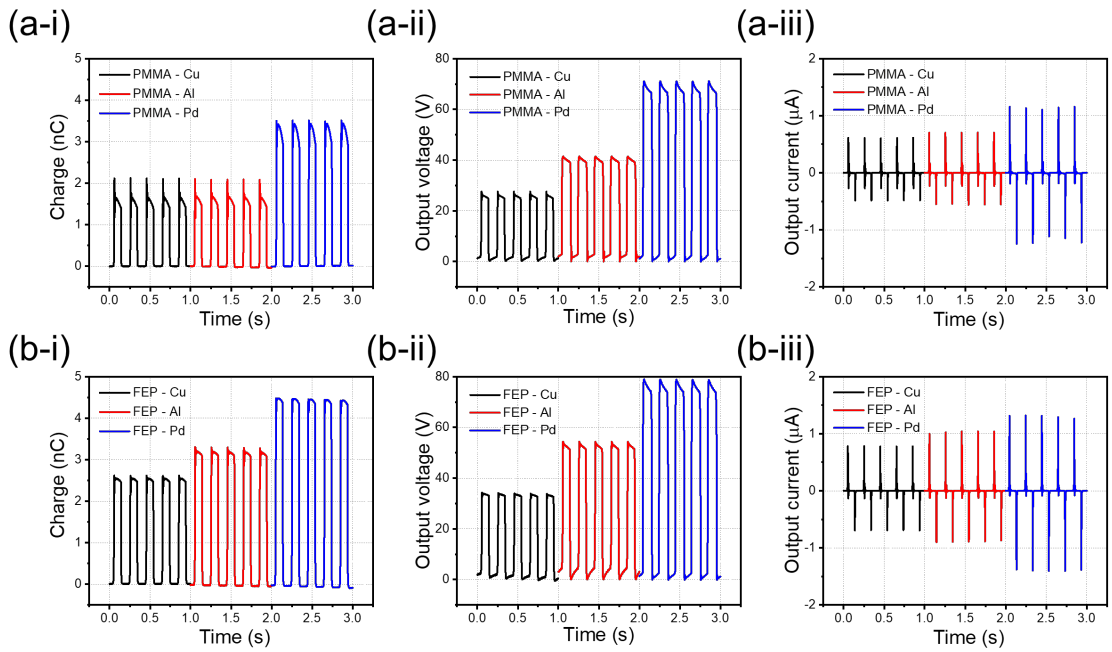

Figure S1. Triboelectric performances obtained for various flat dielectric films and metal electrodes. (a-i) Transferred charge, (a-ii) output voltage, and (a-iii) output current of a TENG comprising a flat PMMA film with different metal electrodes (Cu, Al, and Pd). (b-i) Transferred charge, (b-ii) output voltage, and (b-iii) output current of a TENG comprising a flat fluorinated ethylene propylene (FEP) film with different metal electrodes (Cu, Al, and Pd).

For TENGs comprising a flat PMMA film, the transferred charge obtained for a Pd electrode was 1.6 times higher than that obtained for Cu and Al electrodes. The output voltage and output current were also maximized for the Pd electrode. For TENGs comprising a flat FEP film, the best energy harvesting performance was also observed in the case of the Pd electrode. Therefore, Pd was used as the electrode material to maximize energy-harvesting performance.

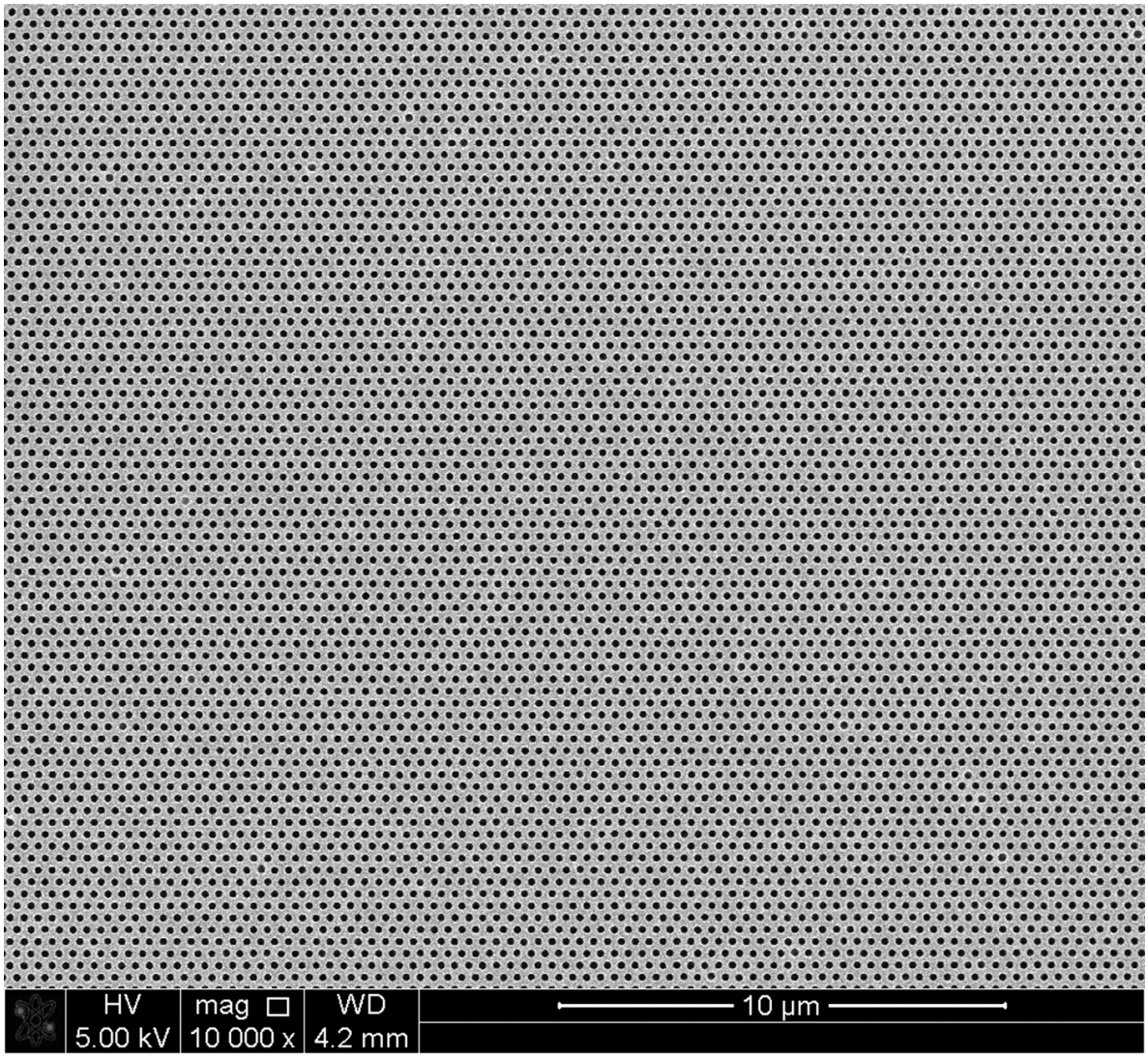

Figure S2. Large-area top-view SEM image of the conductor part of the AR-TENG.

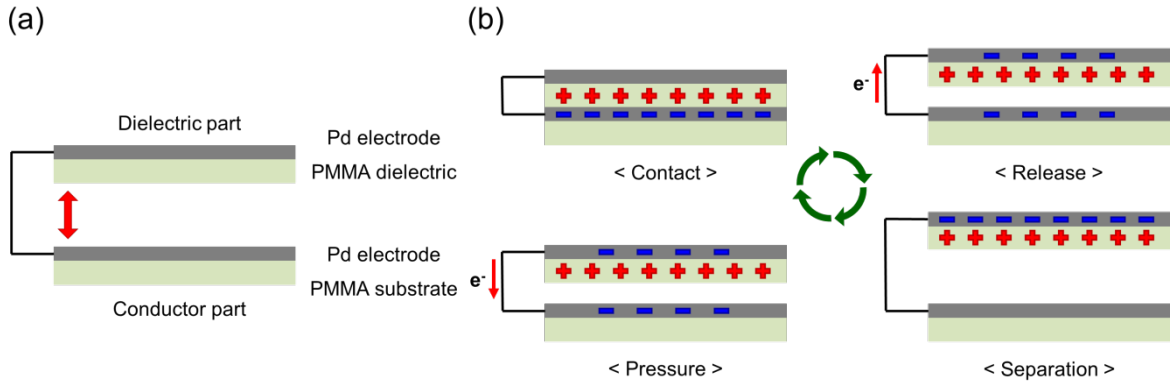

Figure S3. (a) Schematic diagram and (b) working principle of the AR-TENG.

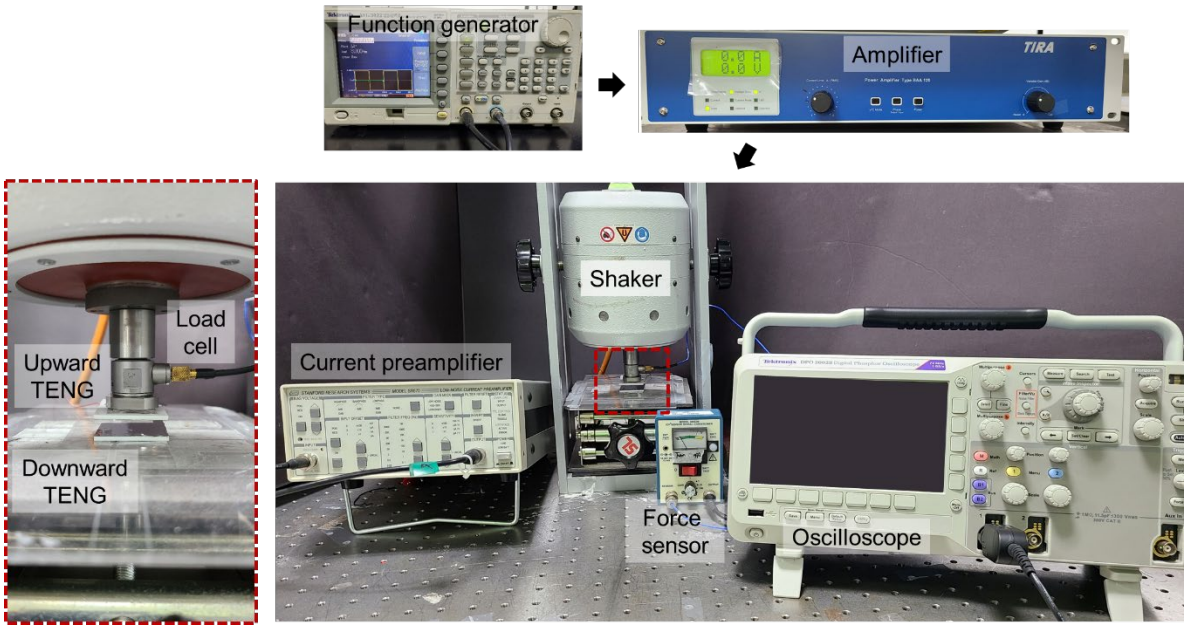

Figure S4. Experimental setup used to characterize the triboelectric performance of the AR-TENG.

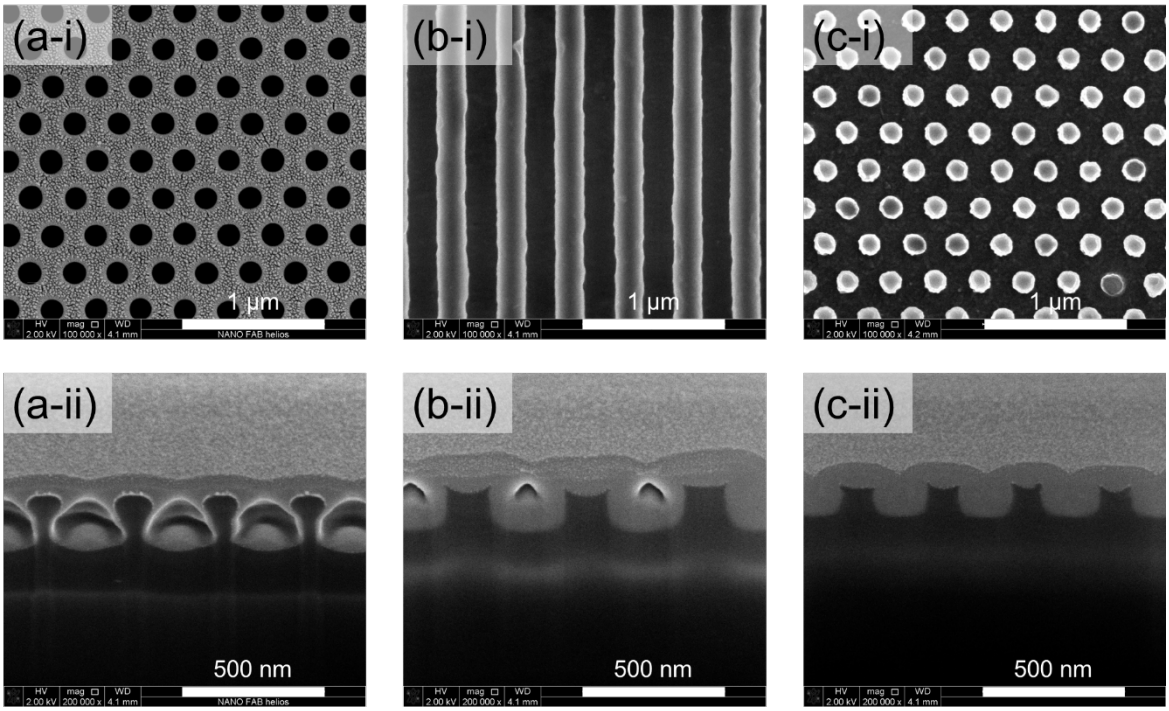

Figure S5. (a-i), (b-i), (c-i) Top- and (a-ii), (b-ii), (c-ii) side-view SEM images of the dielectric part of the AR-TENG with (a) NH, (b) NL, and (c) NP patterns.

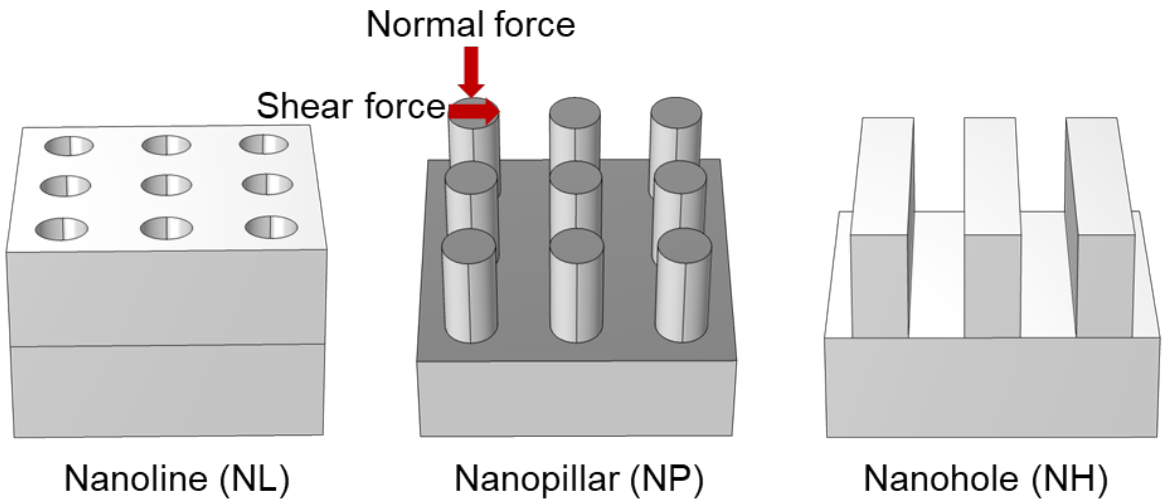

	NL	NP	NH
Diameter or linewidth (nm)	150	150	150
Height (nm)	300	300	300
Pitch (nm)	300	300	300

Simulation parameters	
Applied normal force per unit area	5 MPa
Applied shear force per unit area	5 MPa
Material	PMMA
Young's modulus	2855 MPa
Density	1185 kg/m^3
Poisson's ratio	0.36

Figure S6. Parameters for COMSOL Multiphysics simulation.

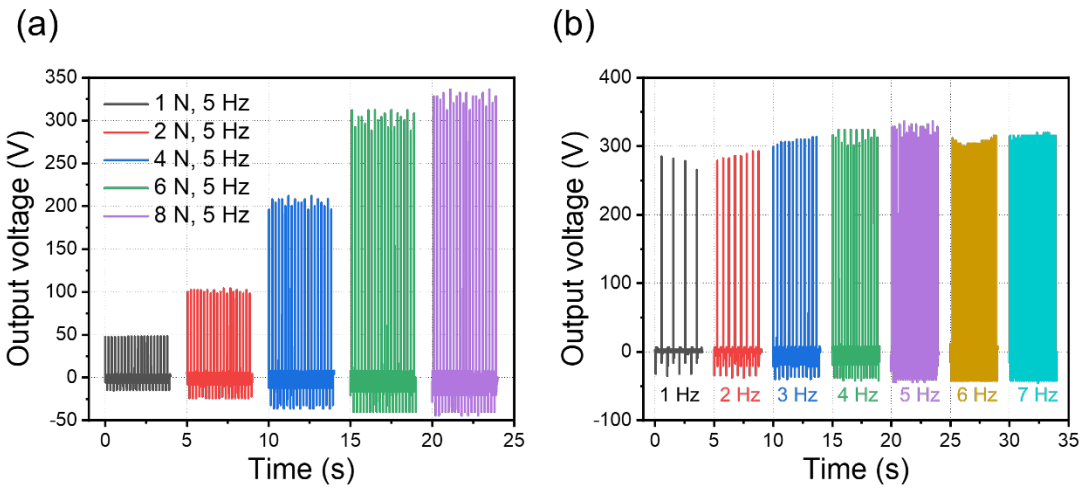

Figure S7. AR-TENG output voltage as a function of (a) the contact force and (b) the vibration frequency of the shaker.

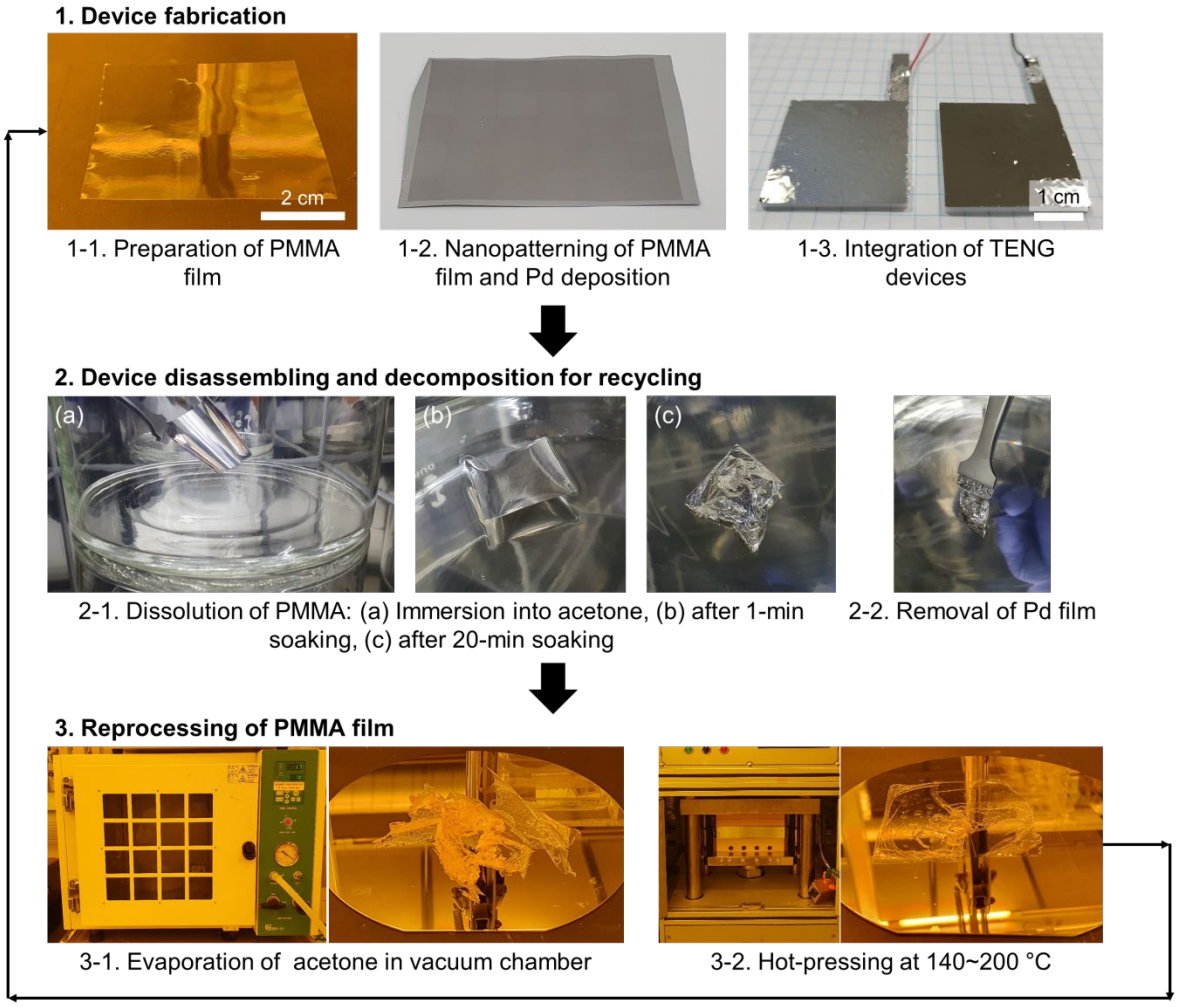

Figure S8. Photographic images corresponding to the different stages of AR-TENG fabrication and recycling.

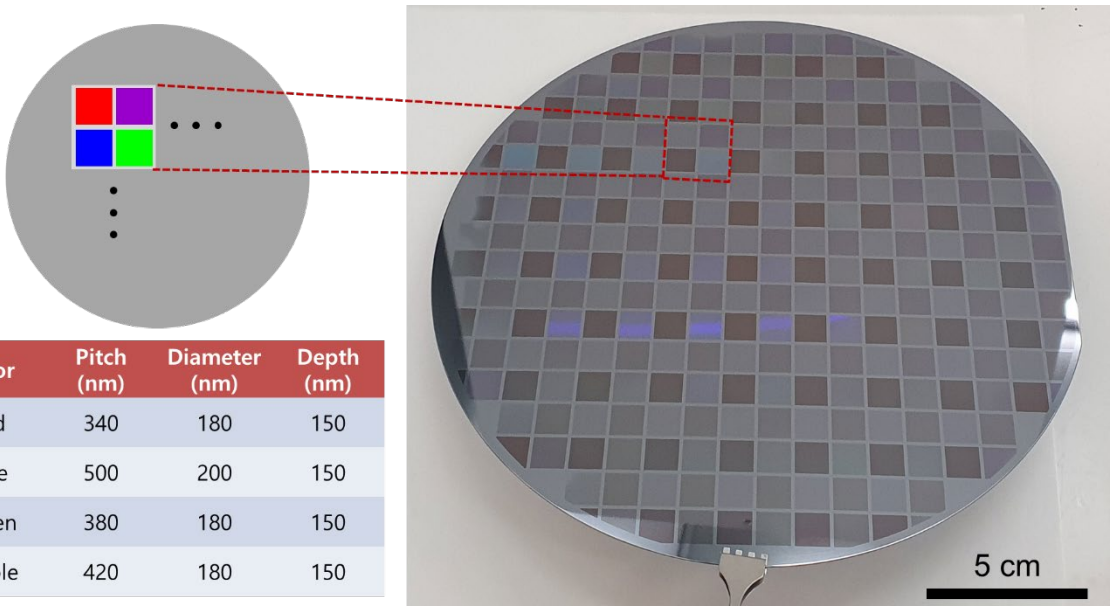

Color	Pitch (nm)	Diameter (nm)	Depth (nm)
Red	340	180	150
Blue	500	200	150
Green	380	180	150
Purple	420	180	150

Figure S9. Si master mold with four different nanohole patterns used to produce the three primary colors of light (red, green, and blue).

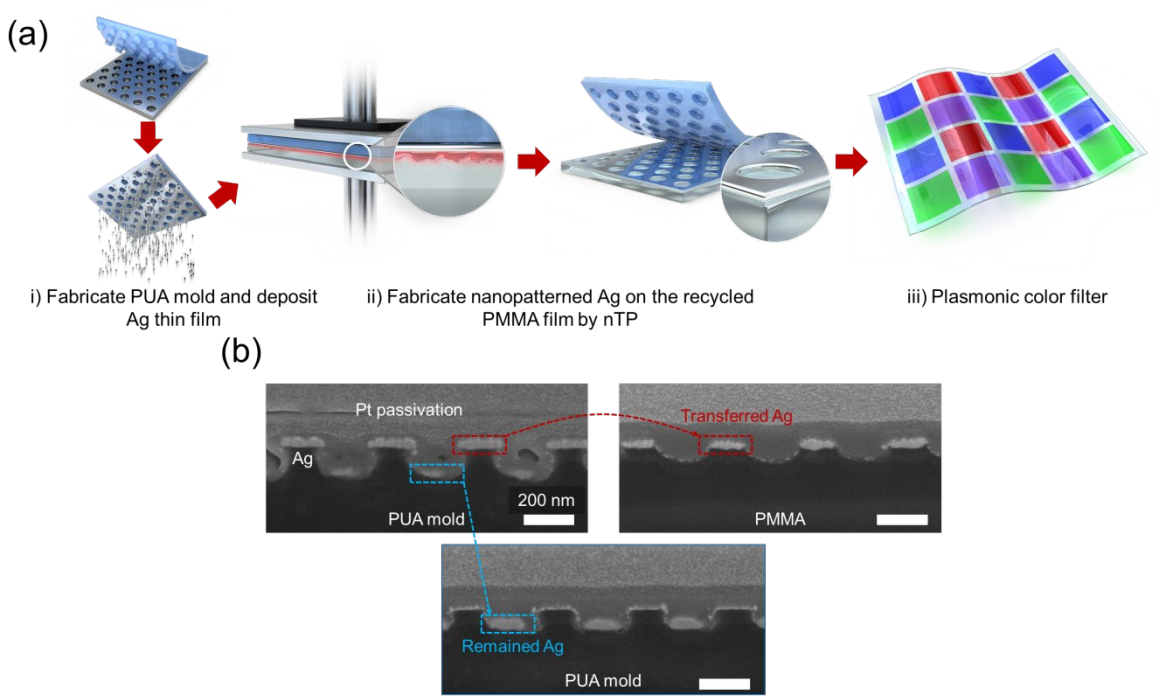

Figure S10. (a) Schematic illustration of PCF fabrication. (b) Side-view SEM images of the PUA mold before and after nTP and of the PMMA film with the transferred Ag NH pattern.

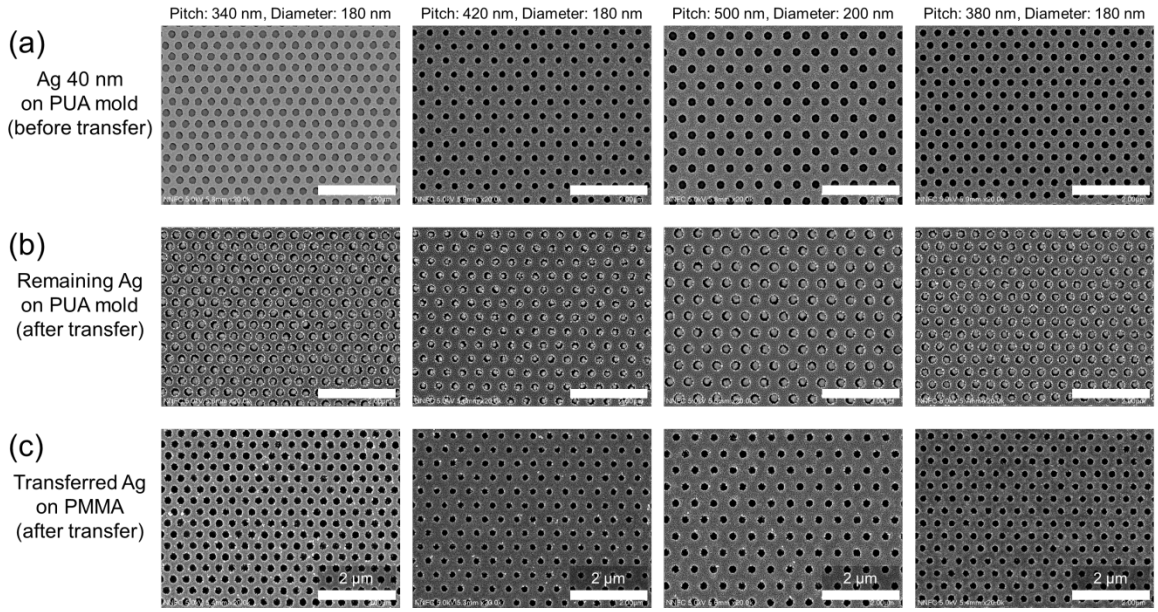

Figure S11. SEM images corresponding to the different steps of nTP.

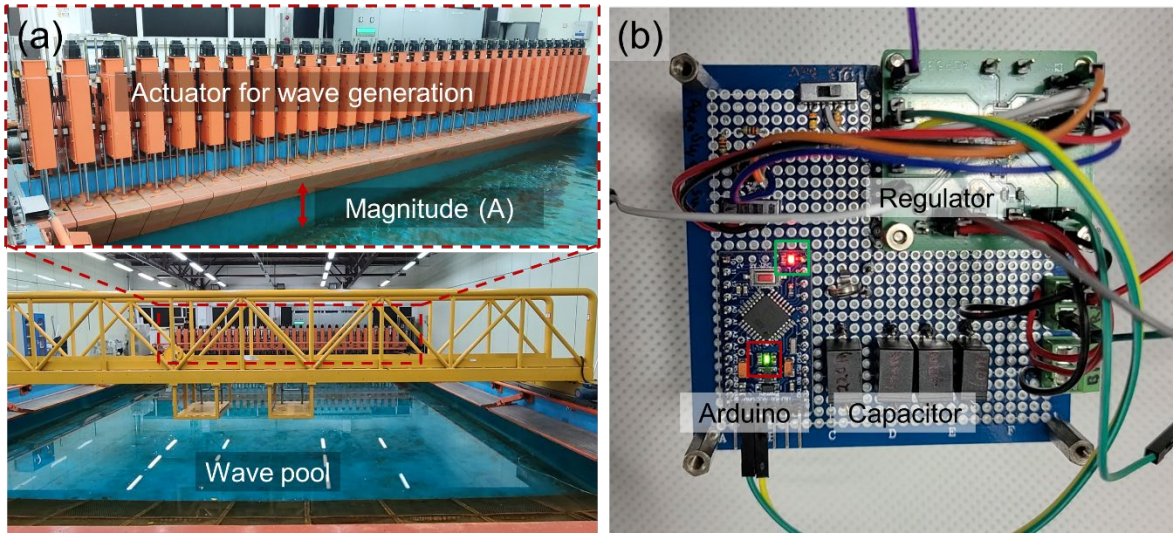

Figure S12. (a) Experimental setup used to mimic the ocean environment and apply wave inputs. (b) Electrical circuit used to charge a commercial Li-ion battery or drive a commercial Arduino board at a constant voltage.

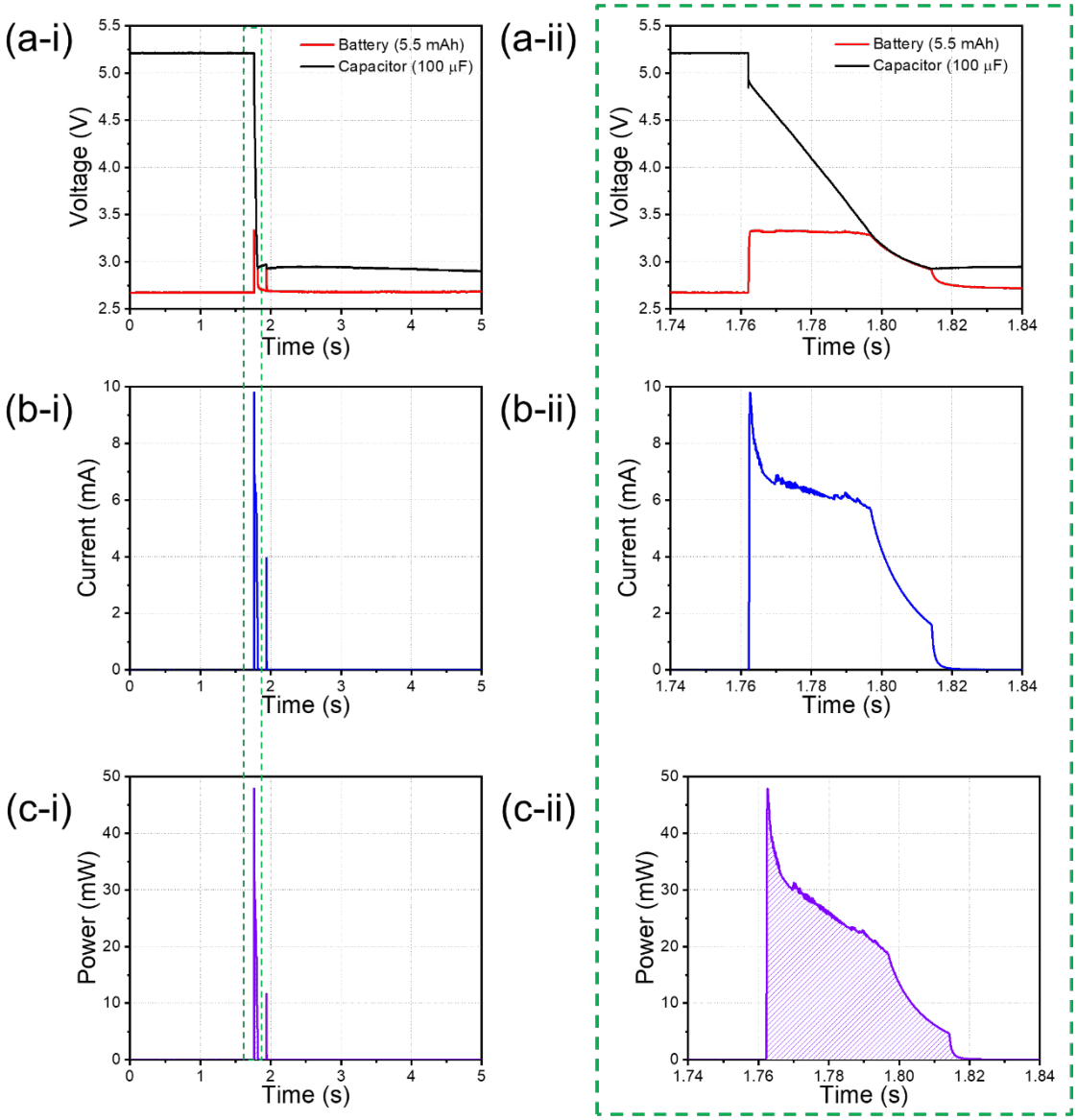

Figure S13. Voltage profiles of the (a-i) capacitor and battery; (b-i) current profile of the regulator; (c-i) calculated total amount of charged power. (a-ii), (b-ii), (c-ii) correspond to the expansions of (a-i), (b-i), and (c-i), respectively.

Supplementary Note 1: Battery Charging Capacity

Figure S13a shows the voltage profiles of the battery and the capacitor while the switch connected to the regulator in the "on" state. When the switch was on, the voltage of the battery stayed constant at 3.3 V (a value corresponding to the output voltage of the regulator), while the voltage of the capacitor dropped from 5.2 V to 3 V. The total energy discharged from the capacitor ($E_{\text{discharged}}$ = 929.81 μW s) was determined as the change in the energy stored in the capacitor before and after discharge.

$$E_{\text{capacitor}} = 0.5CV^2, \quad \text{(S1)}$$

$$E_{\text{discharged}} = 0.5C(V^2_{\text{final}} - V^2_{\text{initial}}), \quad \text{(S2)}$$

where $E_{capacitor}$ is the internal energy of the capacitor, C is the capacitance, and V is the voltage. In addition, to determine the amount of electrical energy transferred to the battery, we first calculated the output power by multiplying the output voltage by the current at the output terminal of the regulator. Thus, the area under the output power–time graph indicates the total amount of electrical energy output from the regulator, that is, the amount of electrical energy transferred to the battery, which was calculated as 908.22 μW s.

$$\int_{Switch\ on}^{Switch\ off} (V(t) \times I(t))dt = \int_{Switch\ on}^{Switch\ off} P(t)dt, \quad \text{(S3)}$$

where $V(t)$, $I(t)$, and $P(t)$ are the time-dependent voltage, current, and power of the regulator, respectively. Therefore, the amount of electrical energy used to drive the regulator was calculated as 21.59 μW s by subtracting the amount of energy transferred to the battery (E_{charged}) from the amount of energy discharged from the capacitor. Hence, the energy efficiency of the circuit (97.7%) was calculated as

$$\eta = E_{\text{charged}}/E_{\text{discharged}}. \quad \text{(S4)}$$

Table S1. Comparison of our AR-TENG with recently reported recyclable/disposable TENGs.

Ref.	TENG structure			Recyclability			Peak output power density ($mW\ m^{-2}$) /Peak-to-peak output voltage (V)
	Total components; triboelectric material (TM) and electrode (E)	Operating mode	Mechanical stability (cyclic test)	Recyclable (R) or disposable (D) components	All-recyclability	Methods or solvents used for recycling	
[S1]	TM: Polyvinyl alcohol (PVA) and sodium alginate E: Li and Al	Contact-separation mode (two electrodes)	N/A	All materials (D)	X	Water	3.8/1.58
[S2]	TM: Kapton and pullulan E: Al and Ag	Contact-separation mode (two electrodes)	10,000	Pullulan (D)	X	Water	41.7/79
[S3]	TM: Biodegradable polymer E: Mg	Contact-separation mode (two electrodes)	N/A	All materials (D)	X	Phosphate-buffered saline	32.6/40
[S4]	TM: Polydimethylsiloxane and Al E: PVA hydrogel and Al	Contact-separation mode (two electrodes)	N/A	PVA (R)	X	Freezing & heating	312.5/200
[S5]	TM: Rice paper E: Conductive ink	Contact-separation mode (single electrode)	10,000	Rice paper (R)	X	Water	376.4/244
[S6]	TM: Calcium alginate and Al E: Al	Contact-separation mode (two electrodes)	2,000	All materials (D)	X	NaCl solution	3.8/33

[S7]	TM: Bacterial cellulose (BC) and BC-CNT-PPy* E: BC-CNT-PPy*	Contact-separation mode (two electrodes)	10,000	All materials (D)	X	Degradation using cellulolytic enzyme	0.83/29
[S8]	TM: VHB tape E: Ionogel	Contact-separation mode (single electrode)	1,000	Ionogel (R)	X	Heating & cooling	67.9/80
This work	TM: PMMA and Pd E: Pd	Contact-separation mode (two electrodes)	200,000	All materials (R)	O	Acetone	1544/360

*BC-CNT-PPy: Bacterial cellulose-carbon nanotube-polypyrrole

References

S1 Q. Liang, Q. Zhang, X. Yan, X. Liao, L. Han, F. Yi, M. Ma, Y. Zhang, *Adv. Mater.*, **2017**, *29*, 1604961.

S2 Y. Lu, X. Li, J. Ping, J.-s. He, J. Wu, *Adv. Mater. Technol.*, **2020**, *5*, 1900905.

S3 Q. Zheng, Y. Zou, Y. Zhang, Z. Liu, B. Shi, X. Wang, Y. Jin, H. Ouyang, Zh. Li, Z. L. Wang, *Sci. Adv.*, **2016**, *2*, e1501478.

S4 W. Xu, L.-B. Huang, M.-C. Wong, L. Chen, G. Bai, J. Hao, *Adv. Energy Mater.*, **2017**, *7*, 1601529.

S5 Y. Chi, K. Xia, Z. Zhu, J. Fu, H. Zhang, C. Du, Zhiwei Xu, *Microelectron. Eng.*, **2019**, *216*, 111059.

S6 Y. Pang, F. Xi, J. Luo, G. Liu, T. Guo., C. Zhang, *RSC Adv.*, **2018**, *8*, 6719.

S7 J. Zhang, S. Hu, Z. Shi, Y. Wang, Y. Lei, J. Han, Y. Xiong, J. Sun, L. Zheng, Q. Sun, G. Yang, Z. L. Wang, *Nano Energy*, **2021**, *89*, 106354.

S8 C. Dang, C. Shao, H. Liu, Y. Chen, H. Qi, *Nano Energy*, **2021**, *90*, 106619.